Available online at www.sciencedirect.com
SCIENCE DIRECT®
Journal of Organometallic Chemistry 689 (2004) 1218–1229
Journal of Organometallic Chemistry
www.elsevier.com/locate/jorganchem

Tetrametallic macrocyclic frameworks constructed from ferrocenedicarboxylato and 2,2′-bipyridine: synthesis, molecular structures and characteristics ☆

Xiangru Meng [a], Hongwei Hou [a,*], Gang Li [a], Baoxian Ye [a], Tiezhu Ge [a], Yaoting Fan [a], Yu Zhu [a], Hiroshi Sakiyama [b]

[a] Department of Chemistry, Zhengzhou University, Henan 450052, PR China
[b] Department of Material and Biological Chemistry, Faculty of Science, Yamagata University, Kojirakawa, Yamagata 900-8560, Japan

Received 6 November 2003; accepted 9 January 2004

Abstract

Four novel tetranuclear macrocyclic compounds $[Cd_2(\eta^2\text{-}O_2CFcCO_2)_2(2,2'\text{-bpy})_2(H_2O)_2]\cdot 2H_2O$ (**1**), $[Zn_2(\eta^2\text{-}O_2CFcCO_2)_2(2,2'\text{-bpy})_2(H_2O)_2]\cdot CH_3OH\cdot H_2O$ (**2**), $[Co_2(O_2CFcCO_2)_2(2,2'\text{-bpy})_2(\mu_2\text{-}OH_2)_2]\cdot CH_3OH\cdot 2H_2O$ (**3**), and $[Ni_2(O_2CFcCO_2)_2(2,2'\text{-bpy})_2(\mu_2\text{-}OH_2)_2]\cdot CH_3OH\cdot 2H_2O$ (Fc = $(\eta^5\text{-}C_5H_4)Fe(\eta^5\text{-}C_5H_4)$) (**4**) have been synthesized and structurally characterized by single crystal diffraction. The magnetic behaviors for compounds (**3**) and (**4**) are studied in the temperature range of 5.0–300 K. The results show that the antiferromagnetic coupling of Co^{II}–Co^{II} pairs occurs in (**3**), and unusual global ferromagnetic coupling between nickel (II) ions exists in (**4**). The solution-state differential pulse voltammetries of compounds (**1**)–(**4**) all show two peaks with large separations (ΔE) that indicate strong interactions between two ferrocene moieties. Their fluorescent and thermal properties were also investigated.

Keywords: Tetranuclear macrocyclic compound; Magnetic properties; Electrochemical properties; Luminescence properties

1. Introduction

Polycarboxyl ligands play an important role in the field of coordination chemistry due to the diversity coordination modes such as monodentate mode, bidentate-bridging mode, bidentate-chelating mode, tridentate-bridging mode, tetradentate-bridging mode and so on. Up to date, a large number of complexes containing carboxylate ligands have been prepared and most of them are polymeric [1–15].

On the other hand, ferrocene is one of the most important compounds not only in the field of organometallic chemistry but also in the field of coordination chemistry. In the viewpoint of constructing functional compounds, it may be interesting to incorporate carboxyl group to ferrocene moiety. In this context, ferrocenedicarboxylic acid or its sodium salt as a very important carboxylate derivative has attracted much attention. It has been exploited as a multifunctional ligand due to the size and the strong inductive effect of ferrocene and the versatile coordination modes of carboxylate anions [16–27]. Scheme 1 illustrates the reported coordination modes of ferrocenedicarboxylate anions. However, so far, most of the coordination frameworks are built by simple ferrocenecarboxylate unit. There are only several reported examples containing ferrocenecarboxylate anions and organic ligands, such as *O*-ferrocenecarbonyl benzoic acid and 4,4′-bipyridine, *O*-ferrocenecarbonyl benzoic acid and 1,2-bis(4-pyridyl)ethane, sodium ferrocenecarboxylate and 1,2-bis(4-pyridyl)ethane, sodium ferrocenecarboxylate and *N*,*N*′-bis(3-pyridylmethyl)thiourea, sodium ferrocenecarboxylate and 4,4′-trimethylene-dipyridine [28,29].

☆ Supplementary data associated with this article can be found, in the online version, at doi:10.1016/j.jorganchem.2004.01.015.

* Corresponding author. Tel./fax: +86-371-7761744.
E-mail address: houhongw@zzu.edu.cn (H. Hou).

0022-328X/$ - see front matter © 2004 Elsevier B.V. All rights reserved.
doi:10.1016/j.jorganchem.2004.01.015

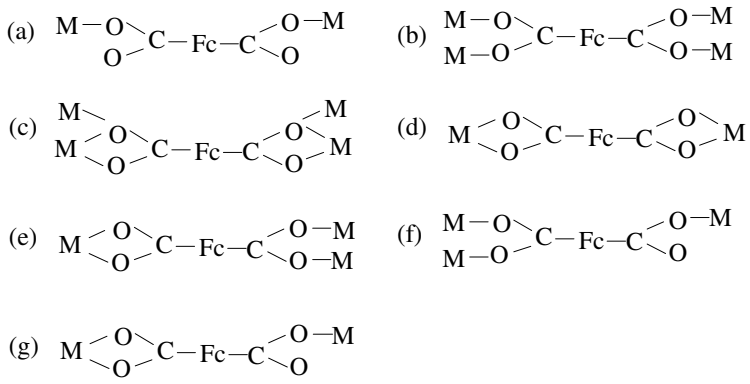

Scheme 1. Typical coordination modes for the ferrocenedicarboxylate ligand.

It is well known that the introduction of chelate ligands such as 2,2′-bpy are capable of "passivating" metal sites via the *N* donors of the organic groups and may induce new structural evolution [30–33]. Our recent efforts are focusing on designing new coordination compounds containing mixed multifunctional ligands and investigating their characteristics. Here, we use 1,1′-ferrocenedicarboxylic acid and 2,2′-bpy to react with $CdCl_2 \cdot 2.5H_2O$, or $ZnCl_2 \cdot 6H_2O$, or $CoCl_2 \cdot 6H_2O$, or $NiCl_2 \cdot 6H_2O$ in the existence of NaOH and obtain four novel tetrametallic macrocyclic frameworks $[Cd_2(\eta^2\text{-}O_2CFcCO_2)_2(2,2'\text{-bpy})_2(H_2O)_2] \cdot 2H_2O$ (**1**), $[Zn_2(\eta^2\text{-}O_2CFcCO_2)_2(2,2'\text{-bpy})_2(H_2O)_2] \cdot CH_3OH \cdot H_2O$ (**2**), $[Co_2(O_2CFcCO_2)_2(2,2'\text{-bpy})_2(\mu_2\text{-}OH_2)_2] \cdot CH_3OH \cdot 2H_2O$ (**3**), and $[Ni_2(O_2CFcCO_2)_2(2,2'\text{-bpy})_2(\mu_2\text{-}OH_2)_2] \cdot CH_3OH \cdot 2H_2O$ (Fc = $(\eta^5\text{-}C_5H_4)Fe(\eta^5\text{-}C_5H_4)$) (**4**). In addition, the electrochemical and fluorescent and thermal properties of compounds (**1**)–(**4**) and the magnetic properties of compounds (**3**) and (**4**) have also been investigated.

2. Results and discussion

2.1. Synthesis

It has been reported that electron-withdrawing substituent on the cyclopentadienyl ring for ferrocene derivatives may provide a greater photolability, and can undergo photolysis in some solvents to cause both ring-metal and ring-carbonyl cleavages, giving Fe^{2+} cation and some free radicals [34–38]. If the mixture of metal ions, 2,2′-bpy, 1,1′-ferrocenedicarboxylic acid and NaOH in methanol–water solution are under light, it could turn from orange to dark-brown solution and then produce brown precipitate, whose composition cannot be identified, compounds (**1**)–(**4**) could not be obtained. So, single crystals suitable for X-ray crystallography for (**1**)–(**4**) were obtained in the dark. The formations of compounds (**1**)–(**4**) are shown in Scheme 2.

All the four complexes are stable in the air. They are not soluble in common organic solvents, such as MeOH, EtOH, MeCN, and THF, but just soluble in high-polar solvents DMSO or DMF.

2.2. Crystal structure of $[Cd_2(\eta^2\text{-}O_2CFcCO_2)_2(2,2'\text{-bpy})_2(H_2O)_2] \cdot 2H_2O$ (1)

The crystal structure analysis by X-ray diffraction demonstrates that compound (**1**) exhibits a tetrametallic macrocyclic framework, where two Cd(II) centers (with the Cd1–Cd1A distance of 5.156 Å) bridged by two ferrocenedicarboxylate anions (with the Fe1–Fe1A distance of 10.138 Å). The four coplanar metals Cd1, Cd1A, Fe1, and Fe1A form a slightly distorted rhombus with the sides of 5.440 Å (Cd1–Fe1A and Cd1A–Fe1) and 5.924 Å (Cd1–Fe1 and Cd1A–Fe1A) and the

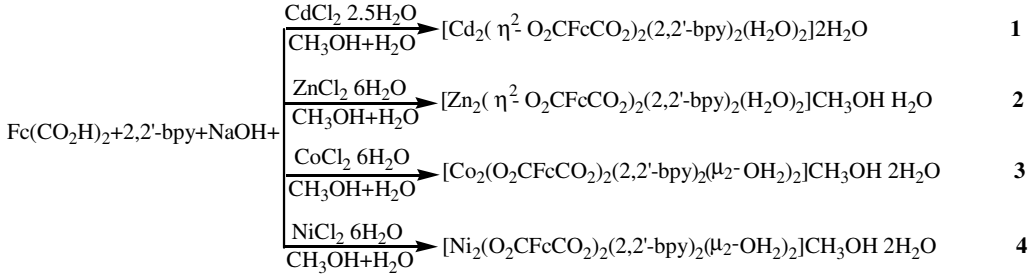

Scheme 2.

interior angles of 53.8° and 126.2°, respectively. The carboxyl groups are deprotonated, in agreement with the IR data in which no strong absorption peaks around 1678 cm^{-1} for COOH are observed. This molecule crystallizes in the space group $P\bar{1}$. The perspective view of (**1**) together with the atomic numbering scheme is illustrated in Fig. 1(a).

Each cadmium atom is coordinated by six donors, two nitrogen atoms from one chelate 2,2′-bpy ligand, one oxygen atom from coordination water molecular and three oxygen atoms belonging to two ferrocenedicarboxylato groups. Around the central Cd(II) atom, the bond lengths of Cd1–N are 2.334(4) and 2.360(5) Å, respectively; the bond lengths of Cd1–O are in the range of 2.281(4)–2.426(5) Å; the O5–Cd1–N1 bond angle (176.33(18)°) is close to 180°; O1A, O2A, O3, N2, and Cd1 atoms are nearly co-planar (the mean deviation from plane is 0.2188 Å). So the local environment around the Cd(II) atom can be best described as a distorted octahedron geometry. It should be noted that the

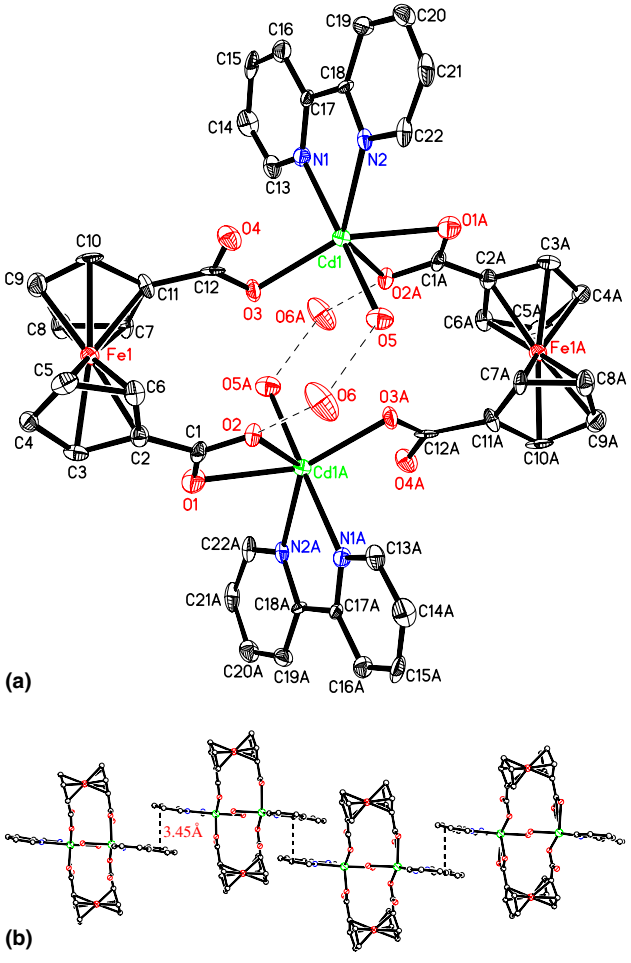

Fig. 1. (a) Perspective view of compound (**1**) with atom labeling scheme. The hydrogen atoms are omitted for clarity. (b) View of one-dimensional chain in compound (**1**) showing the intermolecular π–π interactions.

two 2,2′-bpy ligands are equivalent; the two ferrocenedicarboxylato ligands are equivalent too. In each 2,2′-bpy, the dihedral angle between two pyridine rings is 8.9°. In each ferrocenyl moiety, cyclopentadienyl rings are planar and nearly parallel with a dihedral angle of 2.7°, the intra C–C distances range from 1.414(9) to 1.437(9) Å, which are close to those observed in 1,1′-ferrocenedicarboxylic acid. Furthermore, in every ferrocenedicarboxylato moiety (such as in Fe1 moiety), one carbonyl group as bidentate-chelating fashion coordinates to Cd1A, another carbonyl group as monodentate fashion binds to Cd1. The coordination modes are different from those reported tetrametallic compounds [Zn(1,1′-ferdc)(1-methylimidazole)$_2$]$_2$ [39] and [Cu(1,1′-ferdc)(Py)(DMF)(H_2O)]$_2$(1,1′-H_2ferdc = 1,1′-ferrocenedicarboxylic acid) [25], in which all the carbonyl groups are monodentate fashion. The overall conformation of the ferrocenedicarboxylato moiety in compound (**1**) can be regarded as a synclinal (staggered) conformation with the torsion angle for the moiety being 49.6°, which is similar to that in [Zn(1,1′-ferdc)(1-methylimidazole)$_2$]$_2$ [39], and different from the synperiplanar conformation of free 1,1′-ferrocenedicarboxylic acid (the torsion angle of the disubsituted ferrocene is 0.3°) and [Cu(1,1′-ferdc)(Py)(DMF)(H_2O)]$_2$ (the torsion angle of the disubsituted ferrocene is 0.1°) [25].

There are two kinds of hydrogen bonds in (**1**), one is between O6 (from the crystallized water molecule) and O2 (from the bidentate-chelating coordinated carboxyl), and the other is between O6 and O5 (from coordinated water molecule). These hydrogen bonds stabilize the heterotetrametallic rings. The O6–O2 and O6–O5 distances are 2.771 and 2.834 Å, respectively.

We also found that pyridine rings between adjacent tetrametallic units are arranged in almost parallel fashion (the dihedral angle between the pyridine rings is 8.9°) with the interplanar distance of av. 3.45 Å. Tetrametallic macrocyclic units are linked one by one by these π–π interactions forming one-dimensional infinite chains (Fig. 1(b)).

*2.3. Crystal structure of [$Zn_2(\eta^2$-$O_2CFcCO_2)_2(2,2'$-bpy$)_2(H_2O)_2]\cdot CH_3OH\cdot H_2O$ (**2**)*

The crystal structure of compound (**2**) is similar to (**1**). It contains two kinds of tetrametallic $Zn_2(\eta^2$-$O_2CFcCO_2)_2(2,2'$-bpy$)_2(H_2O)_2$ groups. Each Zn1 ion is bonded to two nitrogen atoms from one chelate 2,2′-bpy ligand and four oxygen atoms from one coordination water molecular and two ferrocenedicarboxylato groups to furnish a significantly distorted octahedron geometry. Around Zn1 ion, O1A, O2A, O3, and N2 atoms are nearly co-planar (the mean deviation from plane is 0.1302 Å), the O5–Zn1–N1 bond angle (170.21(17)°) is close to 180°, two Zn1–N bond lengths are nearly equal (Zn1–N1 = 2.174(5) Å, Zn1–N2 = 2.173(4) Å, and the

four Zn1–O bond lengths are 1.916(4), 2.103(4), 2.132(4), and 2.363(4) Å, respectively. Two Zn1 atoms are linked by two bridging $O_2CFcCO_2^{2-}$ leading to a centrosymmetric tetrametallic ring. In the ring, the four coplanar atoms Zn1, Zn1A, Fe1, and Fe1A form a slightly distorted rhombus with the sides of 5.202 and 5.687 Å and the interior angles of 52° and 128°, respectively. The Zn1–Zn1A and Fe1–Fe1A distances are 4.793 and 9.790 Å, respectively. The dihedral angle between two pyridine rings from one 2,2′-bpy ligand is 7.8°.

Around Zn2 ion, O6A, O7A, O8, and N3 atoms are nearly co-planar (the mean deviation from plane is 0.0216 Å), the O10–Zn2–N4 bond angle is 171.52(16)°, the Zn2–N bond lengths (2.002(4) and 2.132(4) Å) are shorter than those of Zn1–N, the Zn2–O bond lengths are ranging from 2.082(4) to 2.463(5) Å. In the tetrametallic macrocycle $(Zn2)_2(O_2CFcCO_2)_2(2,2'\text{-bpy})_2(H_2O)_2$, Zn2, Zn2A, Fe2, and Fe2A are coplanar and form a slightly distorted rhombus with the sides of 5.313 and 5.846 Å and the interior angles of 51.2° and 128.8°, respectively. The Zn2–Zn2A and Fe2–Fe2A distances (4.842 and 10.67 Å) are slightly longer than those in $(Zn1)_2(O_2CFcCO_2)_2(2,2'\text{-bpy})_2(H_2O)_2$ unit. The dihedral angle between two pyridine rings of one 2,2′-bpy ligand is 3.6°; the cyclopentadienyl rings from the same ferrocenyl moiety are nearly parallel with a dihedral angle of 2.0°. But the overall conformation of the ferrocenedicarboxylato moiety is different from that in $(Zn1)_2(O_2CFcCO_2)_2(2,2'\text{-bpy})_2(H_2O)_2$ unit and compound (**1**), it is regarded as a synclinal (eclipsed) conformation with the torsion angle of 59.3°.

Separated discrete molecular units $(Zn1)_2(O_2CFcCO_2)_2(2,2'\text{-bpy})_2(H_2O)_2$, H_2O, CH_3OH, and $(Zn2)_2(O_2CFcCO_2)_2(2,2'\text{-bpy})_2(H_2O)_2$ are linked orderly by three kinds of O–H···O hydrogen bonds leading to one-dimensional infinite chains (Fig. 2). The O1B–O11C(W), O11C(W)–O12A(CH_3OH) and O12A(CH_3OH)–O9A separations are 2.721, 2.598 and 2.665 Å, respectively. Pyridine rings between adjacent two $(Zn1)_2(O_2CFcCO_2)_2(2,2'\text{-bpy})_2(H_2O)_2$ are arranged in face to face fashion with the av. distance of 3.49 Å, and pyridine rings between adjacent two $(Zn2)_2(O_2CFcCO_2)_2(2,2'\text{-bpy})_2(H_2O)_2$ units are stacked with interplanar distance of av. 3.60 Å. Although the π–π interactions are weak, these kinds of interactions are important in the molecular assembly.

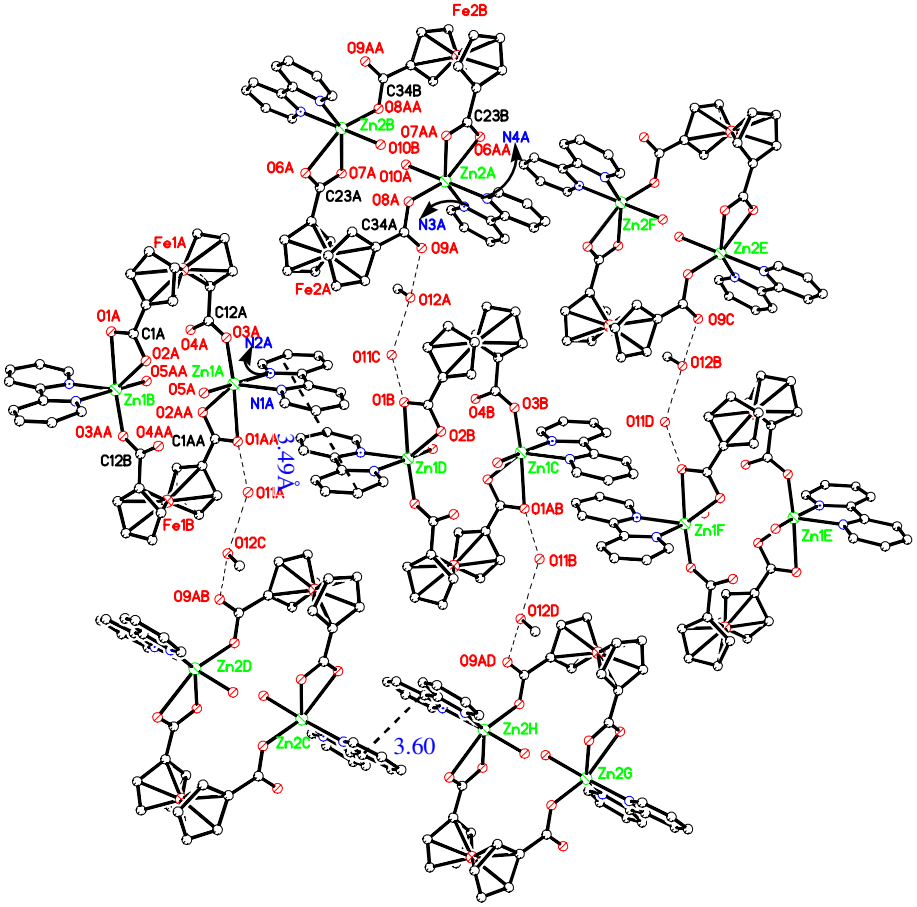

Fig. 2. View of one-dimensional chain in compound (**2**) showing the π–π interactions between the chains.

2.4. Crystal structure of $[Co_2(O_2CFcCO_2)_2(2,2'\text{-bpy})_2(\mu_2\text{-}OH_2)_2]\cdot CH_3OH\cdot 2H_2O$ (3)

The crystal structure of compound (**3**) is different from those of (**1**) and (**2**). Two cobalt atoms are bridged by two oxygen atoms from two coordination water molecules forming a slightly distorted rhombus (Co1–O5–Co1A–O5A) with the sides of 2.122 and 2.229 Å and the interior angles of 79.20° and 100.80°. At the same time, two cobalt atoms are also bridged by two $O_2CFcCO_2^{2-}$ ligands leading to a slightly distorted rhombus (Co1–Fe1–Co1A–Fe1A) with the sides of 5.654 and 5.712 Å and the interior angles of 34.3° and 145.7°, respectively. So the separation between Co1 and Co1A (3.013 Å) is obviously shorter than those of Cd1–Cd1A, Zn1–Zn1A, and Zn2–Zn2A, but the Fe1–Fe1A distance (10.860 Å) is longer than those in compounds (**1**) and (**2**). The two rhombus planes are arranged at almost right angle (the dihedral angle between the two planes is 91.2°).

Each cobalt atom is at a six-coordinated geometry in which two nitrogen atoms come from one 2,2′-bpy ligand, four oxygen atoms from two ferrocenedicarboxylate ligands and two coordinated water molecules, respectively. The distances of Co1–O are ranging from 2.053(2) to 2.229(2) Å, the Co1–N distances are 2.092(3) and 2.136(3) Å, respectively. N1, N2, O5, O5A, and Co1 are nearly coplanar (the mean deviation from plane is 0.0246 Å), and the bond angle of O1A–Co1–O4 (176.05(8)°) is close to 180°.

The dihedral angle between the two pyridine rings is 6.2°, the cyclopentadienyl rings are nearly parallel with the dihedral angle of 1.4°. The carbonyl groups have the same monodentate coordination mode, which is similar to those reported Zn(II) and Cu(II) tetrametallic compounds, [25,39] but different from those in compounds (**1**) and (**2**). The overall conformation of the ferrocenedicarboxylato moiety can be regarded as a synperiplanar conformation with the torsion angle for the moiety being 13.2°, which is similar to the synperiplanar conformations of 1,1′-ferrocenedicarboxylic acid, but different from the synclinal conformation of ferrocene moiety in compounds (**1**) and (**2**).

Furthermore, two adjacent $Co_2(O_2CFcCO_2)_2(2,2'\text{-bpy})_2(\mu_2\text{-}OH_2)_2$ units are bridged by two H_2O molecules through the O–H···O hydrogen bonds resulting to one-dimensional infinite chains (Fig. 3). The O3AA–O7A(W) and O7A(W)–O1B separations are 2.823 and 2.900 Å, respectively.

2.5. Crystal structure of $[Ni_2(O_2CFcCO_2)_2(2,2'\text{-bpy})_2(\mu_2\text{-}OH_2)_2]\cdot CH_3OH\cdot 2H_2O$ (4)

Compound (**4**) has the same structure as compound (**3**). Two nickel atoms are bridged by two oxygen atoms from two coordination water molecules as well as bridged by two $O_2CFcCO_2^{2-}$ ligands forming two slightly distorted rhombus (Ni1–O5–Ni1A–O5A and Ni1–Fe1–Ni1A–Fe1A) with the sides of 2.108, 2.138 and 5.628, 5.680 Å, respectively. The distance between Ni1 and Ni1A (3.249 Å) is longer than that of Co1–Co1A.

Each nickel atom is coordinated by two nitrogen atoms from one 2,2′-bpy ligand and four oxygen atoms from two coordinated water molecules and two ferrocenedicarboxylate ligands. The bond lengths of Ni1–N (2.043(3) and 2.084(3) Å) are slightly shorter than those of Co1–N, and the Ni1–O bonds lengths are in the range 2.047(3)–2.138(3) Å. Ni1, N1, N2, O5, and O5A are nearly coplanar (the mean deviation from plane is 0.0191 Å), and the bond angle of O1–Ni1–O3A (179.33(11)°) is close to 180°.

In compound (**4**), the coordination modes of the two carbonyl groups as well as the overall conformation of ferrocenedicarboxylato moieties (synperiplanar conformation with the torsion angle of 13.1°) are the same as

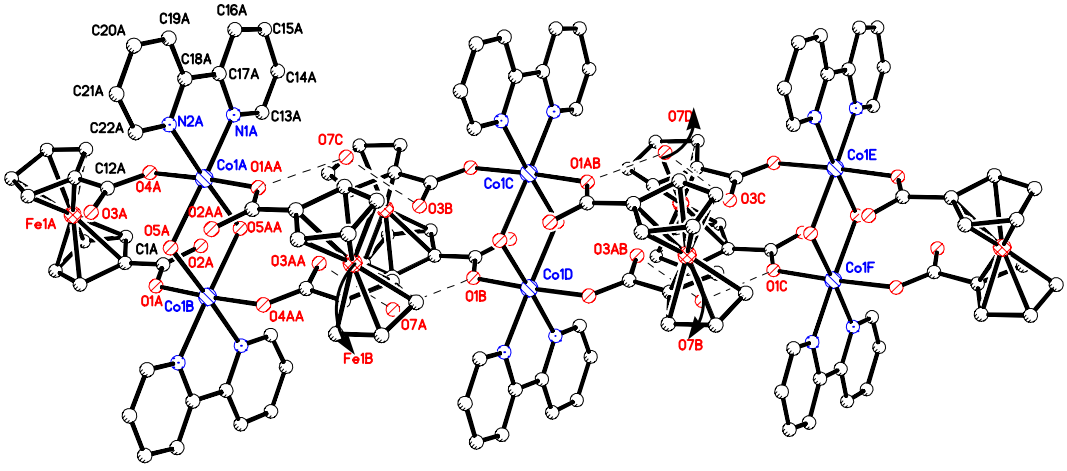

Fig. 3. View of one-dimensional chain in compound (**3**) showing the intermolecular hydrogen bonds.

those in compound (**3**). In addition, the presence of hydrogen bonds among $Ni_2(O_2CFcCO_2)_2(2,2'\text{-bpy})_2(\mu_2\text{-}OH_2)_2$, CH_3OH and H_2O stabilize the heterotetrametallic ring.

2.6. IR spectroscopy

The infrared spectra of compounds (**1**)–(**4**) are quite similar. The band belonging to H_2O occurs at 3418 cm^{-1} for (**1**), 3372 cm^{-1} for (**2**), 3435 cm^{-1} for (**3**), and 3432 cm^{-1} for (**4**). The bands in 3085–3096 and 487–495 cm^{-1} regions are the characteristic IR bands of the ferrocenyl group, which are close to the previous reported compounds [40–42]. The characteristic absorption of 2,2′-bpy are observed as four strong or medium bands in 1563–1571, 1384–1393, 1017–1028, and 772–798 cm^{-1} ranges. The strong absorption bands at 1563–1571 and 1384–1393 cm^{-1} ranges can be assigned to $v_{as}(COO^-)$ and $v_s(COO^-)$ vibrations, respectively, which is consistent with the known complexes [43–45].

2.7. Thermogravimetric analysis (TGA)

The TG-DTA of compounds (**1**)–(**4**) was determined in the range of 20–1000 °C in air. The TG curve of compound (**1**) exhibits three continuous weight loss stages in the ranges 73–160, 212–324 and 324–392 °C, corresponding to the concomitant release of the crystallized water and coordinated water molecules, and the decomposition of 2,2′-bpy and $Fc(COO)_2^{2-}$ anions. Finally, a plateau region is observed from 392 to 1000 °C. A brown amorphous residue of $2CdO + Fe_2O_3$ (observed 36.82%, calculated 36.11%) is remained. There are one weak endothermic peak (142 °C) and two very strong exothermic peaks (282 and 364 °C) in the DTA curve of (**1**). The TG curve of compound (**2**) shows that it loses weight from 46 to 212 °C corresponding to the losses of solvent molecules (H_2O, CH_3OH) and the coordinated water, then keeps losing weight from 212 to 314 °C corresponding to the losses of 2,2′-bpy, and finally loses weight from 314 to 428 °C corresponding to the decomposition of the $Fc(COO)_2^{2-}$ anions. One weak endothermic peak (184 °C) and two strong exothermic peaks (304 and 378 °C) in the DTA curve also record the weight loss processes of various groups. One endothermic peak (176 °C) and two exothermic peaks (297 and 381 °C) can also be observed in the DTA curve of compound (**3**), it first loses the solvent molecules (H_2O, CH_3OH) and the coordinated water from 41 to 211 °C, secondly goes through weight loss steps in the temperature ranges of 211–324 and 324–417 °C corresponding to the decomposition of 2,2′-bpy and the $Fc(COO)_2^{2-}$ anions. The DTA curve of compound (**4**) is similar to that of compound (**3**). There are also one endothermic peak (168 °C) and two exothermic peaks (256 and 368 °C) in the DTA curve of compound (**4**). The weight losing from 56 to 206 °C is corresponding to the departure of the H_2O and CH_3OH, the weight losing from 236 to 288 °C is corresponding to the decomposition of the 2,2′-bpy, and the weight losing from 288 to 384 °C is corresponding to the decomposition of the $Fc(COO)_2^{2-}$ anions.

2.8. Photoluminescent properties

The photoluminescent properties were investigated in the solid state at room temperature. Compared with the free 1,1′-ferrocenedicarboxylic acid, the fluorescent intensities of the compounds (**1**)–(**4**) are slightly weakened. Their luminescent spectra as well as 1,1′-ferrocenedicarboxylic acid are shown in Fig. 4. Excitation at 241 nm leads to broad violet-fluorescent emission bands at 390 nm for (**1**), 392 nm for (**2**), 393 nm for (**3**), and 391 nm for (**4**), which are near to the maximum emission at 390 nm for 1,1′-ferrocenedicarboxylic acid under the same conditions. Therefore, the emissions observed in compounds (**1**)–(**4**) are neither MLCT (metal-to-ligand charge transfer) nor LMCT (ligand-to-metal charge transfer) in nature, and can tentatively be assigned to the intraligand fluorescent emission. In our previous paper, similar photoluminescences have been reported for the two-dimensional layered polymers $\{[M(\eta^2\text{-}O_2CFcCO_2\text{-}\eta^2)(\mu_2\text{-}\eta^2\text{-}O_2CFcCO_2\text{-}\eta^2\text{-}\mu_2)_{0.5}(H_2O)_2]\cdot mH_2O\}_n$ (Fc = $(\eta^5\text{-}C_5H_4)Fe(\eta^5\text{-}C_5H_4)$, $M = Tb^{3+}$, Eu^{3+}, Y^{3+}; $m = 1$ or 2) and one-dimensional wave-shaped polymer $\{[Cd(\eta^2\text{-}O_2CFcCO_2\text{-}\eta^2)(H_2O)_3]\cdot 4H_2O\}_n$ with maximum emission at 393 nm [26].

2.9. Redox properties

The solution-state differential pulse voltammetries of compounds (**1**)–(**4**) and 1,1′-ferrocenedicarboxylic acid are shown in Fig. 5. It can be seen from Fig. 5 that these compounds all show two peaks with half-wave potentials ($E_{1/2}$) at 0.54 and 0.71 V for (**1**), 0.60 and 0.71 V for (**2**), 0.45 and 0.85 V for (**3**), 0.50 and 0.82 V for (**4**),

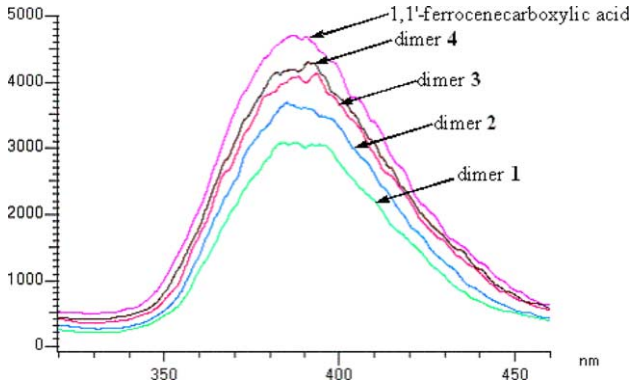

Fig. 4. Emission spectra of 1,1′-ferrocenecarboxylic acid and compounds (**1**)–(**4**) in solid state.

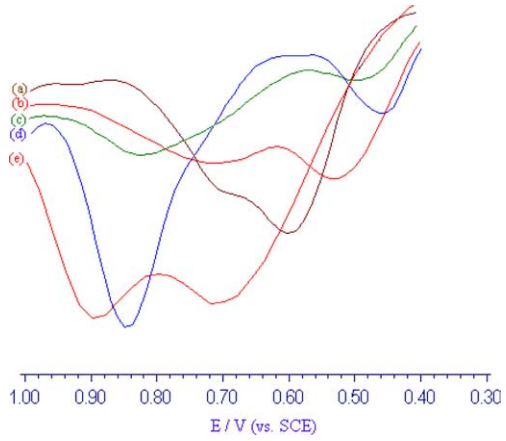

Fig. 5. Differential pulse voltammogram of compounds (**1**) (b), (**2**) (a), (**3**) (d), (**4**) (c) and the 1,1′-ferrocenecarboxylic acid (e) ($\sim 1.0 \times 10^{-3}$ M) in DMF containing n-Bu_4NClO_4 (0.1 M) at a scanning rate of 20 mV s^{-1} (vs. SCE).

and 0.71 and 0.90 V for 1,1′-ferrocenedicarboxylic acid, respectively, corresponding to the two single-electron oxidations of the ferrocenyl moieties. Obviously, the half-wave potentials of (**1**)–(**4**) are shifted to lower potentials compared with those of 1,1′-ferrocenedicarboxylic acid. It is apparent that metal ions Cd(II), Zn(II), Co(II), or Ni(II) have large influence on the half-wave potentials of the ferrocenyl moieties. The ΔE values of ca. 0.17 V for (**1**), 0.11 V for (**2**), 0.40 V for (**3**) and 0.32 V for (**4**) indicate strong interactions between two ferrocene moieties. Similar separations (ΔE) have also been found in compounds Cu_2(1,1′-ferdc)$_2$(Py)$_2$(DMF)$_2$(H_2O)$_2$ ($\Delta E = 0.15$ V) and Ni_2(1,1′-ferdc)$_2$(Py)$_4$(H_2O) ($\Delta E = 0.26$ V) [25].

*2.10. Magnetic properties of [$Co_2(O_2CFcCO_2)_2(2,2'$-$bpy)_2(H_2O)_2$]·CH_3OH ·$2H_2O$ (**3**)*

Variable-temperature magnetic study on compound (**3**) was carried out over the temperature range 5.0–300 K. The temperature dependence of χ_M^{-1} and $\chi_M T$ per Co is depicted in Fig. 6. The thermal evolution of χ_M^{-1} obeys Curie–Weiss law, $\chi_M = C/(T-\theta)$ over the whole temperature range with Weiss constant, θ, of −3.61 K and the Curie constant, C_M, of 2.92 cm^3 K mol^{-1}. The effective magnetic moment per metal atom at room temperature, 4.81 μ_B, is larger than the spin-only value of high-spin cobalt (II) (3.87 μ_B, $\mu_{SO} = [4S(S+1)]^{1/2}$; $S = 3/2$) but close to the value expected when the spin momentum and orbital momentum exist independently [5.20 μ_B, $\mu_{LS} = [L(L+1)+4S(S+1)]^{1/2}$; $L = 3, S = 3/2$]. This indicates that an important contribution of the orbital angular momentum typical for the $^4T_{1g}$ ground term is involved. From 300 to 46 K, the magnetic moments decrease with the decreasing temperature implying the existence of an antiferromagnetic coupling between the paramagnetic Co(II) centers. On further

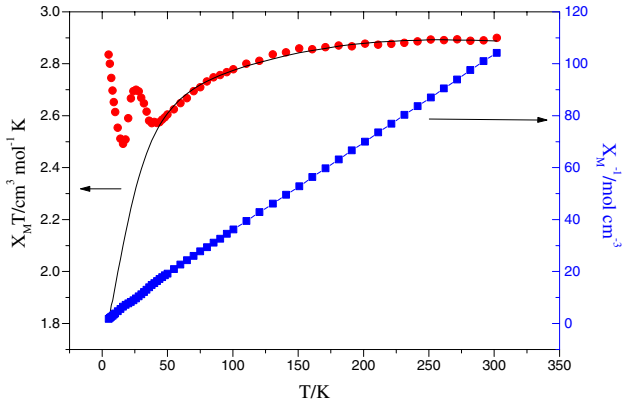

Fig. 6. Plots of χ_M^{-1} and $\chi_M T$ vs. T for (**3**). Solid line is theoretical curve obtained with $\lambda = -80$, $\kappa = 0.94$, $\Delta = 440$ and $J = 0$ cm^{-1}.

decreasing the temperature below 46 K, there is a strange up-down-up behavior. This deviation below 46 K is mainly due to the impurity. One possibility is a mixing of transmetallated species such as [Fe_2(O_2 $CFcCO_2$)$_2$(2,2′-bpy)$_2$(H_2O)$_2$]·CH_3OH ·$2H_2O$. Another possibility is a mixing of metal oxide or metal from spatula and so on. Very small amount of the paramagnetic impurity causes a deviation.

In order to further investigate the interaction between Co^{II} and Co^{II} ions, we use the magnetic equations reported by Hiroshi Sakiyama et al. [46] to analyze our experimental data. The data were well simulated in the temperature range 46–300 K, and the calculated curve is also shown in Fig. 6. Fitting parameters were $\lambda = -80$, $\kappa = 0.94$, $\Delta = 440$ and $J = 0$ cm^{-1}. The g values were calculated as $g_z = 2.16$ and $g_x = 4.94$. The discrepancy factor $R = [\sum(\chi_{obs} - \chi_{calc})^2 / \sum(\chi_{obs})^2]^{1/2}$ in the least-squares fits is 1.99×10^{-5}.

The spin–orbit coupling λ for Co(II) ions is theoretically expected to be −172 cm^{-1}, but the λ value for compound (**3**) is much smaller than −172 cm^{-1}. The orbital reduction factor κ means the reduction of the orbital momentum caused by the delocalization of the unpaired electrons, but it also contains the admixture of the upper $^4T_{1g}(^4P_1)$ state into $^4T_{1g}(^4F_1)$ ground state. In the free Co(II) ion, κ is known to be ∼0.93 [47,48]. Known values of the axial splitting parameter Δ are in the range 200–800 cm^{-1} [49]. The parameters of κ and Δ obtained for compound (**3**) are normal. The J value of 0 cm^{-1} indicates that the magnetic interaction between the Co(II) ions is very small.

*2.11. Magnetic properties of [$Ni_2(O_2CFcCO_2)_2(2,2'$-$bpy)_2(H_2O)_2$]·CH_3OH ·$2H_2O$ (**4**)*

The variable-temperature magnetic susceptibility measurements were performed in the temperature range of 5.0–300 K. The χ_M^{-1} and $\chi_M T$ vs. T curves are shown in Fig. 7. The thermal evolution of χ_M^{-1} obeys Curie–

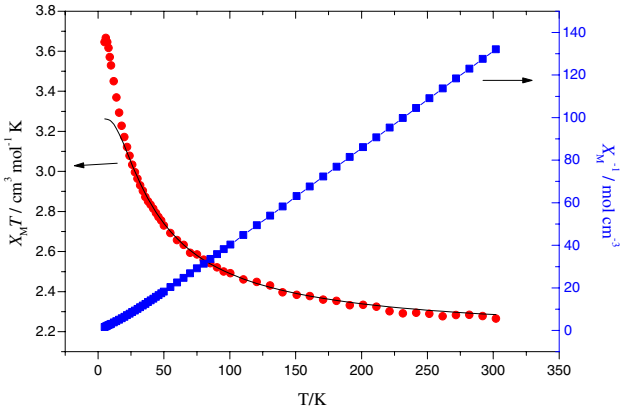

Fig. 7. Plot of χ_M^{-1} and $\chi_M T$ vs. T for (**4**). Solid line is theoretical curve obtained with $g = 2.085, J = 8.15$ cm^{-1}.

Weiss law, $\chi_M = C/(T-\theta)$ over the whole temperature range with Weiss constant, θ, of 7.19 K and the Curie constant, C_M, of 2.238 cm^3 K mol^{-1}. It can be seen from Fig. 7, at 300 K, $\chi_M T$ is equal to 2.265 cm^3 K mol^{-1}, which is close to the value of the reported dinuclear nickel complex $[Ni_2(L\text{–}H)_2][ClO_4]_2(H_2O)$ (L = 2-((bis (2-aminoethyl)amino)methyl)phenol) [50]. When the temperature is lowered from 300 to 5 K, $\chi_M T$ values increased continuously. This behavior indicates an unusual global ferromagnetic coupling between the nickel (II) ions. The effective magnetic moment per metal atom of 3.01 μ_B at room temperature is close to that of the known complex $[Ni_2(L)(N_3)(H_2O)][CF_3SO_3]_3 \cdot 4H_2O$ (L = N[$(CH_2)_2$NHCH$_2$(C_6H_4-*m*)CH_2 NH$(CH_2)_2]_3$N) ($\mu_{eff} = 2.85$ μ_B) [51]. The data have been quantitative analyzed based on the equation [52] deduced from the isotropic spin Hamiltonian operation, $\hat{H} = -2J\hat{S}_1\hat{S}_2$ with quantum numbers $S_1 = S_2 = 1$, χ_M may be expressed by Eq. (1)

$$\chi_M = \frac{2N\beta^2 g^2}{KT}\left[\frac{\exp(2J/KT) + 5\exp(6J/KT)}{1 + 3\exp(2J/KT) + 5\exp(6J/KT)}\right] + N\alpha, \quad (1)$$

where χ_M denotes the susceptibility over binuclear complexes, $N\alpha$ is temperature independent paramagnetism ($N\alpha = 200 \times 10^{-6}$ cm^3 mol^{-1}) and the other symbols have their usual meaning. The experimental data were well simulated in the temperature range 20–300 K and the calculated curve is also given in Fig. 7. The best-fit parameters are $J = 8.15$ cm^{-1}, $g = 2.085$. The discrepancy factor $R = [\sum(\chi_{obs} - \chi_{calc})^2 / \sum(\chi_{obs})^2]^{1/2}$ in the least-squares fits is 7.89×10^{-6}.

Researchers have studied the relationship between the Ni–O–Ni bridging angle and the magnetic behavior, and pointed out that the antiferromagnetic or ferromagnetic exchange interactions are influenced by the Ni–O–Ni bridging angles involved in the superexchange pathway [53–55]. The ferromagnetic behavior of compound (**4**) can be explained by the presence of Ni–O–Ni bridging angle of 99.83° and the accidental orthogonality of the magnetic orbital. The compounds with large Ni–O–Ni angle always show antiferromagnetic behavior with the exchange coupling constant $J < 0$, for example, $[Ni_2(L1)(py)_2](ClO_4)_2$ (L1 = tetraaminediphenol macrocyclic ligand; 105.7°) [56], $[Ni_2(L2)im]_2](ClO_4)_2$ (L2 = tetraamino diphenol macrocyclic ligand; 105.7°), $[Ni_2(L2)(MeOH)_2(ClO_4)_2] \cdot 2NHEt_3ClO_4$ (101.3°), $[Ni_2(L2)(H_2O)_4](ClO_4)_2 \cdot 4NH_2CONH_2$ (99.5°), $[Ni_2(L2)(NCS)_2(H_2O)_2] \cdot 2Me_2NCHO$ (99.2°). The ferromagnetic behavior with the exchange coupling constant $J > 0$ often appears in the compounds with smaller Ni–O–Ni angle, for example, dinuclear nickel(II) complexes $[Ni_2(L3)(NCS)_3(MeOH)]$ (HL3 = 2-{*N*-[2-(dimethylamino)ethyl]iminomethyl}-6-{*N*-methyl-*N*-[2-(dimethylamino)ethyl]aminomethyl}-4-bromophenol; 101.5°) [53], $[Ni_2(L4)(OAc)_2] \cdot 10H_2O$ (L4 = 2,6-di(aminomethyl)-4-methylphenol macrocyclic ligand; 95.6°) [54] and $[Ni_2(L5)(\mu\text{-}O_2CCH_2NH_3)(H_2O)_2] \cdot (ClO_4)_2 \cdot 2H_2O$ (L5 = tetraaminediphenol macrocyclic ligand; 93.8°) [57], polynuclear nickel(II) complexes $[Ni(OMe)(salal)(EtOH)]_4$ (salal = salicylaldehydato; 97.7°) [58] and $[Ni(2,2'\text{-bipy})_2(OH)_2(H_2btec)]_{3n}$ (beta = 1,2,4,5-benzenetetracarboxylate; 86.01° and 88.56°) [7].

3. Experimental

3.1. General information and materials

All chemicals were of reagent grade quality obtained from commercial sources and used without further purification. Carbon, hydrogen and nitrogen analyses were carried out on a Carlo-Erba 1106 elemental analyzer. IR data were recorded on a Nicolet NEXUS 470-FTIR spectrophotometer with KBr pellets in the 400–4000 cm^{-1} region.

3.2. Preparation of ligand

1,1′-Ferrocenedicarboxylic acid was prepared according to the literature method [59,60]. Anal. Calcd. for $C_{48}H_{40}Fe_4O_{16}$ (%): C, 52.59; H, 3.68. Found: C, 52.62; H, 3.64. IR (KBr)/cm^{-1}: 3423 m, 3010 w, 1678 s, 1490 s, 1403 s, 1301 s, 1168 s, 1031 m, 839 m, 750 m, 514 m, 488 m.

3.3. Preparation of $[Cd_2(\eta^2\text{-}O_2CFcCO_2)_2(2,2'\text{-bpy})_2(H_2O)_2] \cdot 2H_2O$ (**1**)

A methanol solution of 2,2′-bpy (0.05 mmol, 3 ml) was added into the 2 ml methanol solution of $CdCl_2 \cdot 2.5H_2O$ (0.05 mmol), then 4 ml mixture methanol–water solution of $Fc(CO_2H)_2$ (0.05 mmol) and NaOH (0.1 mmol) was added dropwise to the above mixture. The resulting orange solution was allowed to

stand at room temperature in the dark. Good quality red crystals were obtained after several days. Crystals of (**1**) are stable in the air. Yield: 54%. Anal. Calcd. for $C_{44}H_{40}Cd_2Fe_2N_4O_{12}$: C, 45.82; H, 3.50; N, 4.86. Found: C, 46.02; H, 3.47; N, 4.73%. IR (cm^{-1}, KBr): 3418 m, 3085 w, 1571 s, 1476 s, 1393 s, 1163 s, 1017 m, 772 m, 736 m, 516 m, 495 m.

3.4. Preparation of $[Zn_2(\eta^2\text{-}O_2CFcCO_2)_2(2,2'\text{-}bpy)_2(H_2O)_2]\cdot CH_3OH\cdot H_2O$ (**2**)

The procedure was the same as that for (**1**), except that $ZnCl_2\cdot 6H_2O$ was used instead of $CdCl_2\cdot 6H_2O$. Yield: 62%. Anal. Calcd. for $C_{45}H_{42}Fe_2N_4O_{12}Zn_2$: C, 50.36; H, 3.94; N, 5.22. Found: C, 50.83; H, 4.02; N, 5.17%. IR (cm^{-1}, KBr): 3372 m, 3094 w, 1571 s, 1470 s, 1384 s, 1177 s, 1022 m, 798 m, 769 m, 517 m, 495 m.

3.5. Preparation of $[Co_2(O_2CFcCO_2)_2(2,2'\text{-}bpy)_2(\mu_2\text{-}OH_2)_2]\cdot CH_3OH\cdot 2H_2O$ (**3**)

The procedure was the same as that for (**1**), except that $CoCl_2\cdot 6H_2O$ was used instead of $CdCl_2\cdot 6H_2O$. Yield: 58%. Anal. Calcd. for $C_{45}H_{44}Co_2Fe_2N_4O_{13}$: C, 50.12; H, 4.11; N, 5.20. Found: C, 49.86; H, 4.15; N, 5.13%. IR (cm^{-1}, KBr): 3435 m, 3096 w, 1567 s, 1486 s, 1392 s, 1185 s, 1027 m, 772 m, 754 m, 519 m, 487 m.

3.6. Preparation of $[Ni_2(O_2CFcCO_2)_2(2,2'\text{-}bpy)_2(\mu_2\text{-}OH_2)_2]\cdot CH_3OH\cdot 2H_2O$ (**4**)

The procedure was the same as that for (**1**), except that $NiCl_2\cdot 6H_2O$ was used instead of $CdCl_2\cdot 6H_2O$. Yield: 60%. Anal. Calcd. for $C_{45}H_{44}Fe_2N_4Ni_2O_{13}$: C, 50.20; H, 4.11; N, 5.20. Found: C, 50.46; H, 4.07; N, 5.28%. IR (cm^{-1}, KBr): 3432 m, 3086 w, 1563 s, 1482 s, 1392 s, 1184 s, 1028 m, 775 m, 759 m, 520 m, 492 m.

3.7. Crystal structure determination

All measurements were made on a Rigaku RAXIS-IV imaging plate area detector with graphite monochromated Mo-Kα radiation ($\lambda = 0.71073$ Å). Red single crystals of (**1**) ($0.23\times0.20\times0.19$ mm^3), (**2**) ($0.20\times0.20\times0.20$ mm^3), (**3**) ($0.23\times0.20\times0.20$ mm^3), and (**4**) ($0.22\times0.18\times0.17$ mm^3) were selected and mounted on a glass fiber. All data were collected at a

Table 1
Crystal data and structure refinement for compounds (**1**)–(**4**)

Compounds	(**1**)	(**2**)	(**3**)	(**4**)
Formula	$C_{44}H_{40}Cd_2Fe_2N_4O_{12}$	$C_{45}H_{42}Fe_2N_4O_{12}Zn_2$	$C_{45}H_{44}Co_2Fe_2N_4O_{13}$	$C_{45}H_{44}Fe_2N_4Ni_2O_{13}$
Formula weight	1153.30	1073.27	1078.40	1077.96
Temperature (K)	291(2)	291(2)	291(2)	291(2)
Wavelength (Å)	0.71073	0.71073	0.71073	0.71073
Color	Red	Red	Red	Red
Crystal syst	Triclinic	Triclinic	Triclinic	Triclinic
Space group	$P\bar{1}$	$P\bar{1}$	$P\bar{1}$	$P\bar{1}$
a (Å)	8.9347(18)	12.431(3)	9.1856(18)	9.2193(18)
b (Å)	10.936(2)	16.966(3)	11.628(2)	11.521(2)
c (Å)	12.359(3)	10.847(2)	11.897(2)	11.848(2)
α (deg)	112.65(3)	107.58(3)	99.99(3)	99.65(3)
β (deg)	108.27(3)	98.56(3)	108.79(3)	108.68(3)
γ (deg)	94.63(3)	82.29(3)	109.96(3)	110.23(3)
V (Å^3)	1029.9(4)	2146.9(7)	1071.8(4)	1062.2(4)
Z	1	2	1	1
D_c (g cm^{-3})	1.860	1.660	1.671	1.685
Absorption coefficient (mm^{-1})	1.781	1.836	1.497	1.616
F(0 0 0)	576	1096	552	554
Crystal sizes (mm)	$0.23\times0.20\times0.19$	$0.23\times0.20\times0.20$	$0.23\times0.20\times0.20$	$0.20\times0.18\times0.17$
θ range for data collection (deg)	1.93–27.49	1.26–25.00	1.91–27.54	1.91–27.46 ×
Index ranges	$-11\leqslant h\leqslant 11$, $0\leqslant k\leqslant 6$, $-16\leqslant l\leqslant 14$	$0\leqslant h\leqslant 14$, $-19\leqslant k\leqslant 20$, $-11\leqslant l\leqslant 12$	$-11\leqslant h\leqslant 10$, $0\leqslant k\leqslant 15$, $-15\leqslant l\leqslant 15$	$-11\leqslant h\leqslant 10$, $0\leqslant k\leqslant 14$, $-15\leqslant l\leqslant 15$
Reflections collected/unique	2260/2260	5930/5930	3918/3918	3652/3652
Data/restraints/parameters	2260/1/306	5930/0/589	3918/1/321	3652/4/314
Goodness-of-fit on F^2	1.076	1.026	1.081	1.006
Final R indices [$I>2\sigma(I)$]	$R_1 = 0.0313$ $wR_2 = 0.0769$	$R_1 = 0.0494$ $wR_2 = 0.1293$	$R_1 = 0.0363$ $wR_2 = 0.0909$	$R_1 = 0.0431$ $wR_2 = 0.1058$
R indices (all data)	$R_1 = 0.0398$ $wR_2 = 0.0793$	$R_1 = 0.0667$ $wR_2 = 0.0667$	$R_1 = 0.0481$ $wR_2 = 0.0944$	$R_1 = 0.0607$ $wR_2 = 0.1123$

temperature of 291(2) K using the ω-2θ scan technique and corrected for Lorentz-polarization effects. A correction for secondary extinction was applied.

The four structures were solved by direct methods and expanded using the Fourier technique. The non-hydrogen atoms were refined with anisotropic thermal parameters. Hydrogen atoms were included but not refined. The final cycle of full-matrix least squares refinement was based on 2260 observed reflections and 306 variable parameters for (**1**), 5930 observed reflections and 589 variable parameters for (**2**), 3918 observed reflections and 321 variable parameters for (**3**), and 3652 observed reflections and 314 variable parameters for (**4**). All calculations were performed using the SHELX-97 crystallographic software package [61]. Crystal data and experimental details for compounds compounds (**1**)–(**4**) are contained in Table 1. Selected bond lengths and bond angles are listed in Table 2. Electronic supplementary information available: the structural units of compounds (**2**)–(**4**).

3.8. Determination of TGA–DTA

TGA–DTA measurements were performed by heating the sample from 20 to 1000 °C at a rate of 10 °C min^{-1} in air on a Perkin–Elmer DTA-7 differential thermal analyzer.

3.9. Determination of photoluminescent properties

The luminescent spectra were measured on powder samples at room temperature using a model F-4500 Hitachi Fluorescence Spectrophotometer. The excitation slit was 5 nm and the emission slit was 5 nm too, the response time was 2 s.

3.10. Determination of differential pulse voltammetry

Differential pulse voltammetry studies were recorded with a CHI650 electrochemical analyzer utilizing the three-electrode configuration of a Pt working electrode,

Table 2
Selected bond lengths (Å) and angles (deg) for compounds (**1**)–(**4**)

*Polymer (**1**)*[a]			
Cd(1)–O(3)	2.281(4)	Cd(1)–O(5)	2.305(5)
Cd(1)–N(2)	2.344(4)	Cd(1)–N(1)	2.360(5)
Cd(1)–O(2)#1	2.379(4)	Cd(1)–O(1)#1	2.426(5)
O(3)–Cd(1)–O(5)	92.84(17)	O(3)–Cd(1)–N(2)	134.57(17)
O(5)–Cd(1)–N(2)	107.34(18)	O(3)–Cd(1)–N(1)	87.31(16)
O(5)–Cd(1)–N(1)	176.33(18)	N(2)–Cd(1)–N(1)	70.16(17)
*Polymer (**2**)*[b]			
Zn(1)–O(3)	1.916(4)	Zn(1)–O(5)	2.103(4)
Zn(1)–N(1)	2.174(5)	Zn(1)–O(1)#1	2.363(4)
Zn(2)–N(3)	2.002(4)	Zn(2)–O(8)	2.082(4)
Zn(2)–O(10)	2.215(4)	Zn(2)–O(6)#2	2.463(5)
O(3)–Zn(1)–O(5)	91.74(17)	O(3)–Zn(1)–N(2)	102.54(17)
O(5)–Zn(1)–N(2)	96.60(17)	O(2)#1–Zn(1)–N(2)	137.47(16)
O(3)–Zn(1)–N(1)	86.67(18)	O(5)–Zn(1)–N(1)	170.21(17)
N(3)–Zn(2)–O(7)#2	144.14(19)	O(8)–Zn(2)–O(7)#2	96.91(16)
N(3)–Zn(2)–N(4)	80.15(18)	O(8)–Zn(2)–N(4)	101.70(16)
O(7)#2–Zn(2)–N(4)	93.82(17)	N(3)–Zn(2)–O(10)	92.00(16)
*Polymer (**3**)*[c]			
Co(1)–O(4)	2.053(2)	Co(1)–O(1)#1	2.086(2)
Co(1)–N(1)	2.092(3)	Co(1)–O(5)#1	2.122(3)
Co(1)–N(2)	2.136(3)	Co(1)–O(5)	2.229(2)
N(1)–Co(1)–N(2)	77.70(11)	O(5)#1–Co(1)–N(2)	177.90(10)
O(4)–Co(1)–O(5)	88.90(10)	O(1)#1–Co(1)–O(5)	87.50(10)
N(1)–Co(1)–O(5)	178.09(11)	O(5)#1–Co(1)–O(5)	79.20(10)
*Polymer (**4**)*[d]			
Ni(1)–N(2)	2.043(3)	Ni(1)–O(3)#1	2.047(3)
Ni(1)–O(1)	2.078(3)	Ni(1)–N(1)	2.084(4)
Ni(1)–O(5)#1	2.108(3)	Ni(1)–O(5)	2.138(3)
N(2)–Ni(1)–O(3)#1	88.21(13)	N(2)–Ni(1)–O(1)	92.35(12)
O(3)#1–Ni(1)–O(1)	179.33(11)	N(2)–Ni(1)–N(1)	79.94(14)
O(1)–Ni(1)–O(5)#1	89.96(13)	N(1)–Ni(1)–O(5)#1	178.18(13)

[a] Symmetry transformations used to generate equivalent atoms in polymer (**1**): $\#1\ -x+1, -y+2, -z+1$.
[b] Symmetry transformations used to generate equivalent atoms in polymer (**2**): $\#1\ -x+1, -y+1, -z+2 \#2\ -x, -y, -z$.
[c] Symmetry transformations used to generate equivalent atoms in polymer (**3**): $\#1\ -x+1, -y+1, -z$.
[d] Symmetry transformations used to generate equivalent atoms in polymer (**4**): $\#1\ -x-1, -y, -z$.

a Pt auxiliary electrode, and a commercially available saturated calomel electrode as the reference electrode with a pure N_2 gas inlet and outlet. The measurements were performed in DMF solution containing tetraethyl ammonium perchlorate (n-Bu_4NClO_4) (0.1 mol dm^{-3}) as supporting electrolyte, which has a 50 ms pulse width and a 20 ms sample width. The potential was scanned from +0.3 to +1.0 V at scan rate of 20 mV s^{-1}.

Caution! *Although no problems were encountered in this work, the salt perchlorates are potentially explosive. They should be prepared in small quantities and handled with care.*

3.11. Determination of magnetic properties

Variable-temperature magnetic susceptibility data were obtained on a SQUID susceptometer (Quantum Design, MPMS-5) in the temperature range 5–300 K with an applied field of 500 G. All data have been corrected for diamagnetism by using Pascal's constants [62].

Acknowledgements

The authors thank the National Natural Science Foundation of China (Nos. 20001006 and 20371042), the Outstanding Young Teacher Foundation of Ministry of Education and Innovation Foundation of Henan Province for financial support.

References

[1] C. Policar, F. Lambert, M. Cesario, I. Morgenstern-Badarau, Eur. J. Inorg. Chem. (1999) 2201.
[2] T. Imai, M. Shimoi, A. Ouchi, Bull. Chem. Soc. Jpn. 60 (1987) 159.
[3] J.M. Rueff, N. Masciocchi, P. Rabu, A. Sironi, A. Skoulios, Eur. J. Inorg. Chem. (2001) 2843.
[4] T.H. Reineke, M. Eddaoudi, M. O'Keeffe, O.M. Yaghi, Angew. Chem. Int. Ed. 38 (1999) 2590.
[5] J.C. Dai, X.T. Wu, Z.Y. Fu, S.M. Hu, W.X. Du, C.P. Cui, L.M. Wu, H.H. Zhang, R.Q. Sun, Chem. Commun. (2002) 12.
[6] O.M. Yaghi, C.E. Davis, G.M. Li, H.L. Li, J. Am. Chem. Soc. 119 (1997) 2861.
[7] Y.G. Li, N. Hao, Y. Lu, E.B. Wang, Z.H. Kang, C.G. Hu, Inorg. Chem. 42 (2003) 3119.
[8] F.D. Rochon, G. Massarweh, Inorg. Chim. Acta 304 (2000) 190.
[9] H. Li, C.E. Davis, T.L. Groy, D.G. Kelley, O.M. Yaghi, J. Am. Chem. Soc. 120 (1998) 2186.
[10] J. Tao, M.L. Tong, X.M. Chen, J. Chem. Soc., Dalton Trans. (2000) 3669.
[11] C.S. Hong, Y. Do, Inorg. Chem. 37 (1998) 4470.
[12] M.J. Plater, M.R.S.J. Foreman, R.A. Howie, J.M.S. Skakel, A.M.Z. Slawin, Inorg. Chim. Acta 315 (2001) 126.
[13] R. Cao, D. Sun, U. Liang, M. Hong, K. Tatsumi, Q. Shi, Inorg. Chem. 41 (2002) 2087.
[14] S.O.H. Gutschke, D.J. Price, A.K. Powell, P.T. Wood, Eur. J. Inorg. Chem. (2001) 2739.
[15] D.Q. Chu, J.Q. Xu, L.M. Duan, T.G. Wang, A.Q. Tang, L. Ye, Eur. J. Inorg. Chem. (2001) 1135.
[16] D.W. Slocum, C.R. Ernst, Adv. Organomet. Chem. 10 (1972) 106.
[17] J.X. Tao, W.J. Xiao, J. Organomet. Chem. 526 (1993) 21.
[18] M.W. Cooke, T.S. Cameron, K.N. Robertson, J.C. Swarts, M.A.S. Aquino, Organometallics 21 (2002) 5962.
[19] W. Uhl, T. Spies, D. Haase, R. Winter, W. Kaim, Organometallics 19 (2000) 1128.
[20] W. Frosch, S. Back, H. Lang, Organometallics 18 (1999) 5725.
[21] S.D. Christie, S. Subramanian, L.K. Thompson, M. Zaworotko, Chem. Commun. (1994) 2563.
[22] D. Guo, H. Mo, C.Y. Duan, F. Lu, Q.J. Meng, J. Chem. Soc., Dalton Trans. (2002) 2593.
[23] D. Guo, B.G. Zhang, C.Y. Duan, X. Cao, Q.J. Meng, J. Chem. Soc., Dalton Trans. (2003) 282.
[24] S.M. Lee, K.K. Cheung, W.T. Wong, J. Organomet. Chem. 506 (1996) 77.
[25] D. Guo, Y.T. Li, C.Y. Duan, H. Mo, Q.J. Meng, Inorg. Chem. 8 (2003) 2519.
[26] X.R. Meng, G. Li, H.W. Hou, H.Y. Han, Y.T. Fan, Y. Zhu, C.X. Du, J. Organomet. Chem. 679 (2003) 153.
[27] H.W. Hou, G. Li, L.K. Li, Y. Zhu, X.R. Meng, Y.T. Fan, Inorg. Chem. 42 (2003) 429.
[28] G. Li, H.W. Hou, L.K. Li, X.R. Meng, Y.T. Fan, Y. Zhu, Inorg. Chem. 42 (2002) 4995.
[29] H.W. Hou, L.K. Li, G. Li, Y.T. Fan, Y. Zhu, Inorg. Chem. 42 (2003) 3501.
[30] P.J. Hagrman, J. Zubieta, Inorg. Chem. 39 (2000) 3252.
[31] P.J. Zapf, R.C. Haushalter, J. Zubieta, Chem. Mater. 9 (1997) 2019.
[32] Y. Lu, E.B. Wang, M. Yuan, G.Y. Luan, Y.G. Li, J. Chem. Soc., Dalton Trans. (2002) 3029.
[33] Y.G. Li, E.B. Wang, H. Zhang, G.L. Luan, C.W. Hu, J. Solid State Chem. 163 (2002) 10.
[34] P. Bergamini, S.D. Martino, A. Maldotti, S. Sostero, O. Traverso, J. Organomet. Chem. 365 (1989) 341.
[35] L.H. Ali, A. Cox, T.J. Kamp, J. Chem. Soc., Dalton Trans. (1973) 1468.
[36] E.K. Heaney, S.R. Logan, Inorg. Chim. Acta 22 (1977) L3.
[37] D.J. Che, G. Li, X.L. Yao, D.P. Zou, J. Organomet. Chem. 568 (1998) 165.
[38] D.J. Che, G. Li, B.S. Du, Z. Zhang, Y.H. Li, Inorg. Chim. Acta 261 (1997) 121.
[39] T.A. Zevaco, H. Görls, E. Dinjus, Polyhedron 17 (1998) 613.
[40] F. Takusagawa, T.F. Koetzle, Acta Crystallogr. B35 (1979) 2888.
[41] T.H. Allen, O. Kennard, Chem. Des. Automat. News 8 (1993) 146.
[42] F.A. Cotton, L.R. Falvello, A.H. Reid Jr., J.H. Tocher, J. Organomet. Chem. 319 (1987) 87.
[43] F. Ribot, P. Toledano, C. Sanchez, Inorg. Chim. Acta 185 (1991) 239.
[44] J.C.G. Bunzli, G.R. Chopin, Lanthanide Probes in Life, Chemical and Earth Sciences, Elsevier, Amsterdam, 1989.
[45] J.P. Costes, F. Nicodéme, Chem. Eur. J. 8 (2002) 3442.
[46] H. Sakiyama, R. Ito, H. Kumagai, K. Inoue, M. Sakamoto, Y. Nishida, M. Yamasaki, Eur. J. Inorg. Chem. (2001) 2027.
[47] M.E. Lines, J. Chem. Phys. 55 (1971) 2977.
[48] W. Low, Phys. Rev. 109 (1958) 256.
[49] B.N. Figgis, M. Gerloch, J. Lewis, F.E. Mabbs, G.A. Webb, J. Chem. Soc. A (1968) 2086.
[50] E. Berti, A. Caneschi, C. Daiguebonne, P. Dapporto, M. Formica, V. Fusi, L. Giorgi, A. Guerri, M. Micheloni, P. Paolli, R. Pontellini, P. Rossi, Inorg. Chem. 42 (2003) 348.

[51] A. Escuer, C.J. Harding, Y. Dussart, J. Nelson, V. McKee, R. Vicente, J. Chem. Soc., Dalton Trans. (1999) 223.
[52] J. Gao, S.L. Ma, C.Y. Jin, D.Z. Liao, Polyhedron 15 (1996) 2633.
[53] T. Koga, H. Furutachi, T. Nakamura, N. Fukita, M. Ohba, K. Takahashi, H. Okawa, Inorg. Chem. 37 (1998) 989.
[54] Y. Aratake, M. Ohba, H. Sakiyama, M. Tadokoro, N. Matsumoto, H. Ôkawa, Inorg. Chim. Acta 212 (1993) 183.
[55] K.K. Nanda, R. Das, L.K. Thompos, K. Venkatsubramanian, P. Paul, K. Nag, Inorg. Chem. 33 (1994) 1188.
[56] K.K. Nanda, R. Das, M.J. Newlands, R. Hynes, E.J. Gabe, K. Nag, J. Chem. Soc., Dalton Trans. (1992) 897.
[57] R. Das, K.K. Nanda, K. Venkatsubramanian, P. Paul, K. Nag, J. Chem. Soc., Dalton Trans. (1992) 1253.
[58] J.E. Andrew, A.b. Blake, J. Chem. Soc. A (1996) 1456.
[59] M.D. Rausch, D.J. Ciappenelli, J. Organomet. Chem. 10 (1967) 127.
[60] Gmelin Handbuch der Anorganische Chemie. Eisen Organische Verbindungen, vol. A3, Springer, Berlin, Germany, 1976, p. 58.
[61] G.M. Sheldrick, SHELXTL-97 Program for Refining Crystal Structure Refinement, University of Göttingen, Germany, 1997.
[62] R.L. Carlin, Magnetochemistry, Springer, Berlin, Heideberg, New York, Tokyo, 1986.